

ARTICLES

Network organization of the human autophagy system

Christian Behrends¹, Mathew E. Sowa¹, Steven P. Gygi² & J. Wade Harper¹

Autophagy, the process by which proteins and organelles are sequestered in autophagosomal vesicles and delivered to the lysosome/vacuole for degradation, provides a primary route for turnover of stable and defective cellular proteins. Defects in this system are linked with numerous human diseases. Although conserved protein kinase, lipid kinase and ubiquitin-like protein conjugation subnetworks controlling autophagosome formation and cargo recruitment have been defined, our understanding of the global organization of this system is limited. Here we report a proteomic analysis of the autophagy interaction network in human cells under conditions of ongoing (basal) autophagy, revealing a network of 751 interactions among 409 candidate interacting proteins with extensive connectivity among subnetworks. Many new autophagy interaction network components have roles in vesicle trafficking, protein or lipid phosphorylation and protein ubiquitination, and affect autophagosome number or flux when depleted by RNA interference. The six ATG8 orthologues in humans (MAP1LC3/GABARAP proteins) interact with a cohort of 67 proteins, with extensive binding partner overlap between family members, and frequent involvement of a conserved surface on ATG8 proteins known to interact with LC3-interacting regions in partner proteins. These studies provide a global view of the mammalian autophagy interaction landscape and a resource for mechanistic analysis of this critical protein homeostasis pathway.

Protein homeostasis in eukaryotes is controlled by proteasomal turnover of unstable proteins via the ubiquitin system and lysosomal turnover of the majority of stable proteins through macroautophagy (referred to hereafter as autophagy)^{1–3}. The autophagy system orchestrates the engulfment of cytoplasmic proteins into a double-lipid bilayer—the autophagosome—and coordinates fusion of the autophagosome with the lysosome/vacuole, where degradation occurs. Autophagy is activated in response to low nutrient availability to provide building blocks for protein synthesis but can also be used to selectively degrade organelles (for example, mitochondria), misfolded and/or aggregated proteins, and infectious agents¹. Defects in autophagy have also been linked to cancer and removal of apoptotic cell corpses^{1,2}.

Autophagy is controlled by pathways that interpret the status of cellular energy (AMP-dependent protein kinase, AMPK), nutrients/amino acids (target of rapamycin, TOR) and growth factors such as insulin. Studies in yeast have revealed four conserved signalling modules encoded by autophagy (ATG) genes that control major steps in the process (Supplementary Fig. 1b–d)^{1–3}. The Atg1p kinase complex (Atg1p–Atg13p–Atg17p)⁴ and its mammalian counterpart, the unc-51 like kinase (ULK1) complex, control early steps in autophagosome formation, and are regulated by nutrient availability via mammalian TOR (mTOR)⁵. The vacuolar protein sorting Vps34p–Vps30p complex, and its mammalian PIK3C3–BECN1 (beclin) counterpart, control production of phosphoinositide signals that facilitate assembly of the incipient autophagosome⁶. A ubiquitin-like protein (UBL) conjugation cascade—composed of the E1 enzyme Atg7p, two E2 enzymes (Atg10p and Atg3p) and two UBLs (Atg8p and Atg12p)—is required for autophagosome maturation and cargo recruitment^{1–3}. Atg12p is conjugated to a lysine residue in Atg5p via the Atg7p–Atg10p cascade, ultimately forming an oligomeric Atg12p–Atg5p–Atg16p complex that promotes conjugation of the carboxy-terminal Gly residue of Atg8p to phosphatidylethanolamine (PE) via Atg3p⁷ (where -- refers to a covalent bond). The Atg5p complex may also

promote incorporation of Atg8p–PE into autophagosomes, allowing Atg8p to promote autophagosome closure and cargo recruitment. Finally, a recycling system containing Atg9p, Atg2p, Atg18p and Atg21p participates in transfer and recycling of components from the isolation membrane, the presumed source of lipids for production of the autophagosome, to the growing autophagosome⁸.

Although modules within the autophagy system are relatively well characterized, much less is known concerning the overall organization of the pathway and to what extent the various functional elements communicate with each other. Moreover, the autophagy system is more complex in mammalian cells, with several ATG proteins having multiple family members, bringing into question their individual roles in the process. For example, whereas Atg8p in yeast is represented by a single gene, the ATG8 family in humans contains six members (microtubule-associated protein-1 light chain 3A (MAP1LC3A), MAP1LC3B, MAP1LC3C, GABA_A receptor-associated protein (GABARAP), GABARAPL1 and GABARAPL2). Although MAP1LC3 proteins and GABARAP are known to be conjugated to PE and incorporated into autophagosomes, GABARAPL1 and GABARAPL2 are largely unstudied and the biological underpinnings of the diversity of ATG8 proteins in mammals are unknown. Furthermore, it is likely that additional ATG proteins not found in yeast will participate in the process in vertebrate cells, such as the recently identified ATG101 protein⁹. Here we report a systematic proteomic analysis of the human autophagy system coupled with a functional analysis of a subset of genes in the pathway, thereby providing a glimpse into the global architecture of the autophagy interaction network (AIN) and a resource for further mechanistic analysis of this pathway.

Proteomics of the autophagy system

Thirty-two human proteins linked to autophagy or vesicle trafficking were retrovirally expressed as Flag-haemagglutinin (HA) fusion

¹Department of Pathology, Harvard Medical School, Boston, Massachusetts 02115, USA. ²Department of Cell Biology, Harvard Medical School, Boston, Massachusetts 02115, USA.

proteins in 293T cells (Supplementary Fig. 1a and Supplementary Table 1). Proteins in anti-HA immune complexes were identified by mass spectrometry (LC-MS/MS). Total spectral counts for each of the 2,553 unique proteins detected were processed using a modified version of the Comparative Proteomics Analysis Software Suite (CompPASS) to identify high-confidence candidate interaction proteins (HCIPs)⁹. CompPASS uses a database of interacting proteins (including data for all baits reported here and an additional 102 unrelated proteins)⁹ and three specificity metrics (WD^N-score, an associated *P*-value and *Z*-score) to identify HCIPs (Methods and Supplementary Fig. 2a-d). To validate and further delineate the network, 33 HCIPs were chosen as secondary baits for reciprocal proteomic analyses based on interconnectivity with primary baits, the presence of functional domains or Gene Ontology (GO) terms linked to cellular processes associated with autophagy, and the apparent specificity of the interaction based on the WD^N-score (Supplementary Fig. 1a). The number of HCIPs did not correlate with bait abundance (Supplementary Fig. 2e), indicating that bait expression level does not unduly bias HCIP number, and that HCIPs can be identified for baits with very low expression levels. In total, we identified 409 non-redundant HCIPs making 751 interactions (Fig. 1 and Supplementary Fig. 3), referred to here as the AIN. Because the cells used are actively undergoing autophagy under the growth conditions used, albeit with lower rates than found upon stimulation (Supplementary Fig. 6g), the AIN reported here is considered to represent the basal autophagy state.

Overview of the AIN

Hierarchical clustering of the AIN revealed the presence of multi-protein complexes as well as baits that appeared to interact with a number of partners in a distributive manner (Supplementary Fig. 3). To visualize the interconnectivity of the AIN, we combined interaction maps for ten functional subnetworks (Fig. 1). As expected, the UBL conjugation machinery subnetwork displayed extensive connectivity with the ATG8 subnetwork. However, we identified 22 interactions that connected individual proteins or established protein complexes with components in distinct subnetworks. This connectivity is further indicated by the identification of 34 proteins that are found in association with 3 or more bait proteins with WD^N-scores >3.0, representing candidate nodes in the network (Supplementary Fig. 5d).

Using BIOGRID, MINT and STRING protein interaction databases, we identified 84 known protein complexes (KPCs), representing 40 known bait-KPC interactions in the raw AIN (Supplementary Fig. 4b). Using tools in CompPASS that collapse known complexes into single nodes, we identified 497 total candidate associations, of which 429 were not present in these databases (Supplementary Fig. 4a, b). Thus, our analysis greatly expands the number of candidate autophagy network proteins.

Twenty-one per cent of the HCIPs in the AIN were enriched in GO process descriptors encompassing vesicle transport, proteolysis, signal transduction and phosphorylation ($P \approx 10^{-5}$ – 10^{-9}) (Supplementary Fig. 5a), accounting for twenty-six per cent of GO

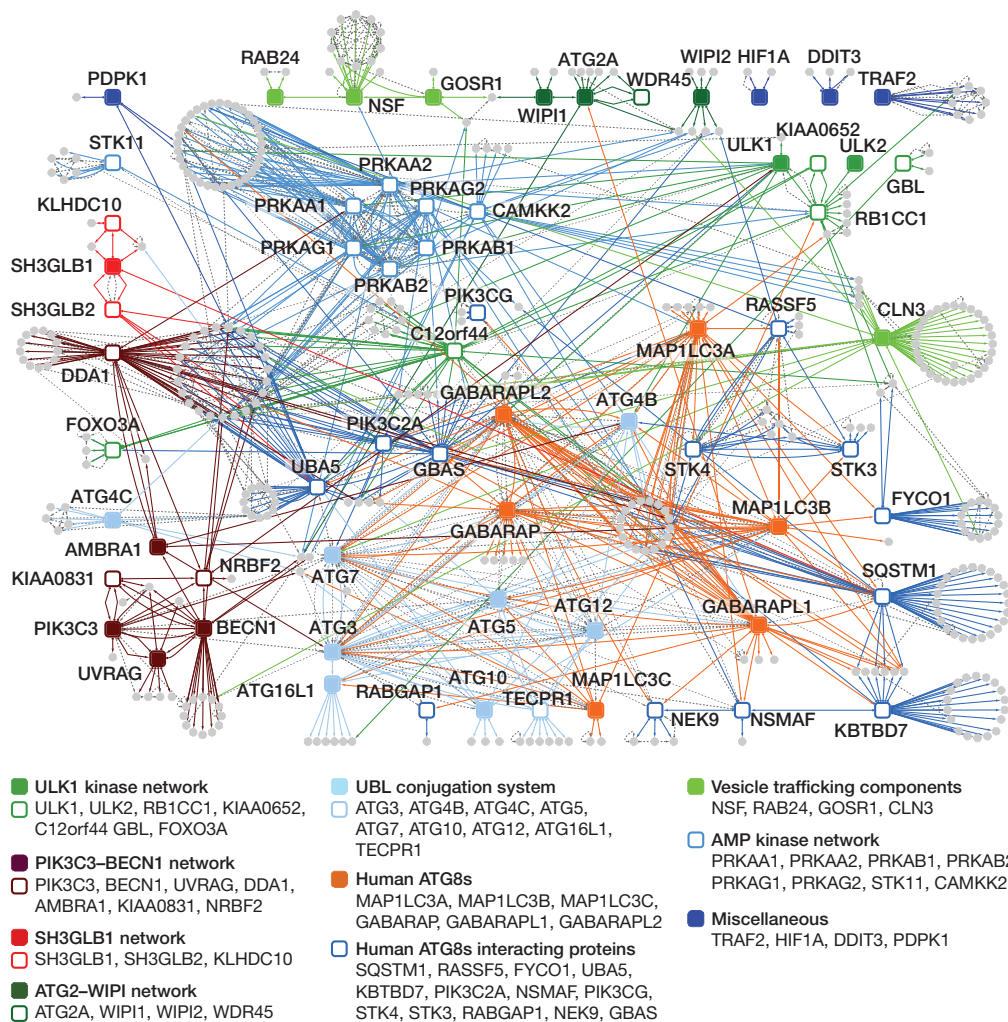


Figure 1 | Overview of the autophagy interaction network (AIN). HCIPs within the autophagy network are shown for 32 primary baits (filled squares) and 33 secondary baits (open squares). Subnetworks are colour-coded. Interacting proteins are indicated by grey circles.

process terms found throughout the AIN HCIPs. Fifty-seven proteins in the AIN lacked GO process descriptors. However, six of these are known autophagy proteins (ATG2A, ATG2B, ATG14, RUBICON, AMBRA1, NBR1), three could be linked to the ubiquitin system, and fourteen could be linked to vesicle or membrane function based on GO component descriptors, functional domains, or previous studies on yeast orthologues (Supplementary Table 7). A variety of functional domains were also enriched ($P \approx 0.05-10^{-7}$), including protein and lipid kinases, G-protein regulatory motifs (TBC), ubiquitin ligase motifs (BTB) and WD40 repeats (Supplementary Fig. 5b, c).

Validation of subnetworks within the AIN

The connectivity within conjugation, ULK1 protein kinase, PIK3C3–BECN1 kinase, ATG2, SH3GLB1 and NSF subnetworks under basal conditions is shown in Fig. 2a–f (see Supplementary Fig. 6e for maps of individual complexes). Of 27 interactions seen between 19 budding yeast Atg proteins found in BIOGRID and MINT, we found 23 corresponding human interactions (Supplementary Fig. 7). The UBL conjugation system is representative of the quality of the interaction data across the larger network. First, the E1 (ATG7) and the ATG8 hydro-lase (ATG4B) associated with six and five ATG8 orthologues, respectively, as well as with ATG12 (Figs 2a and 3a). As in yeast³, ATG5 associated with ATG12, ATG10, ATG16L1, ATG3 and a subset of ATG8 orthologues (Fig. 2a and Supplementary Fig. 7a), supporting

the role of this complex as an ‘E3-like’ activity for ATG8–PE production⁷. In total, 12 of 27 interactions in BIOGRID for the human UBL conjugation system were identified by our proteomics analysis (Supplementary Fig. 6a). The absence of complete representation may reflect the fact that 23 of 27 interactions reported in BIOGRID were from unvalidated high-throughput approaches (Supplementary Fig. 6b). For the UBL conjugation system overall, there were 71 previously unidentified HCIPs, and of the 44 potential reciprocal interactions tested by LC-MS/MS, 47% were validated (Supplementary Fig. 6a). For example, a previously uncharacterized tectonin β-propeller repeat protein, TECPR1, associated reciprocally with ATG12, ATG3 and ATG5 (Fig. 2a and Supplementary Fig. 6f), indicating its involvement in the ATG8 lipidation pathway. The WD40-repeat protein ATG16L1 and TECPR1 also associated with the CCT chaperonin complex implicated in the folding of WD40 proteins¹⁰.

We also identified additional components for other subnetworks. Multiple subunits of the ULK1 and ULK2 kinases were identified, including the recently reported regulatory subunits RB1CC1 (with sequence similarity to Atg11p), KIAA0652 (also called ATG13) and C12orf44 (also called ATG101) (Fig. 2d and Supplementary Fig. 6f)⁵. Moreover, ULK1 and ULK2 associated with catalytic and regulatory subunits of AMPK (Fig. 2d), which are genetically linked to autophagy in yeast and *Drosophila melanogaster*^{11,12}. Similarly, KIAA0831 (also called ATG14) and KIAA0226 (also called RUBICON) were

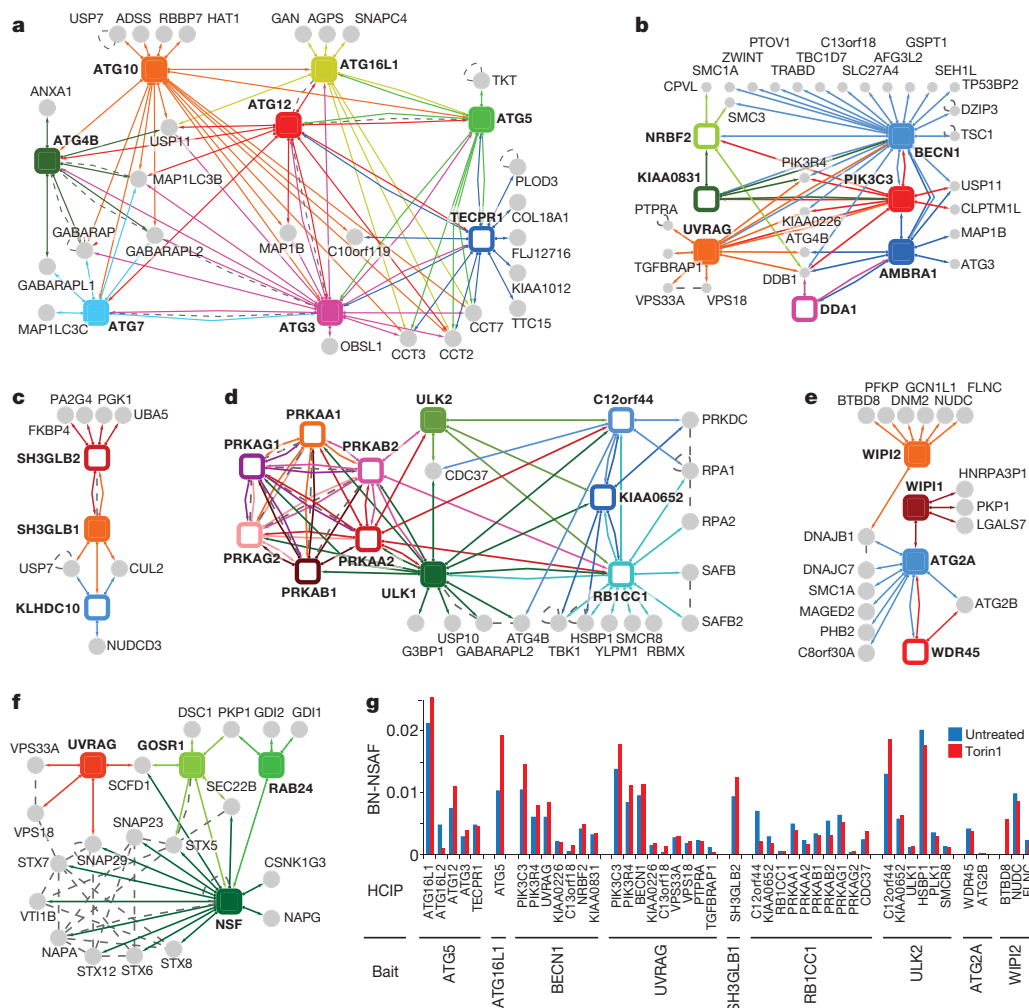


Figure 2 | Autophagy subnetwork maps. Common interacting proteins with subthreshold WD^N-scores were included if HCIP criteria were fulfilled in ≥ 1 IP-MS/MS experiment. Filled squares, primary baits; open squares, secondary baits; grey circles, HCIPs; dotted lines, interactions found in BIOGRID or MINT databases. **a**, UBL transfer cascade network

b, PIK3C3–BECN1 network. **c**, SH3GLB1 network. **d**, ULK1–AMPK network. **e**, ATG2 network. **f**, NSF network. Proteins in bold represent baits used for proteomics. **g**, Effect of autophagy activation by Torin1 on bait–HCIP association. BN-NSAF, bait normalized-normalized spectral abundance factor.

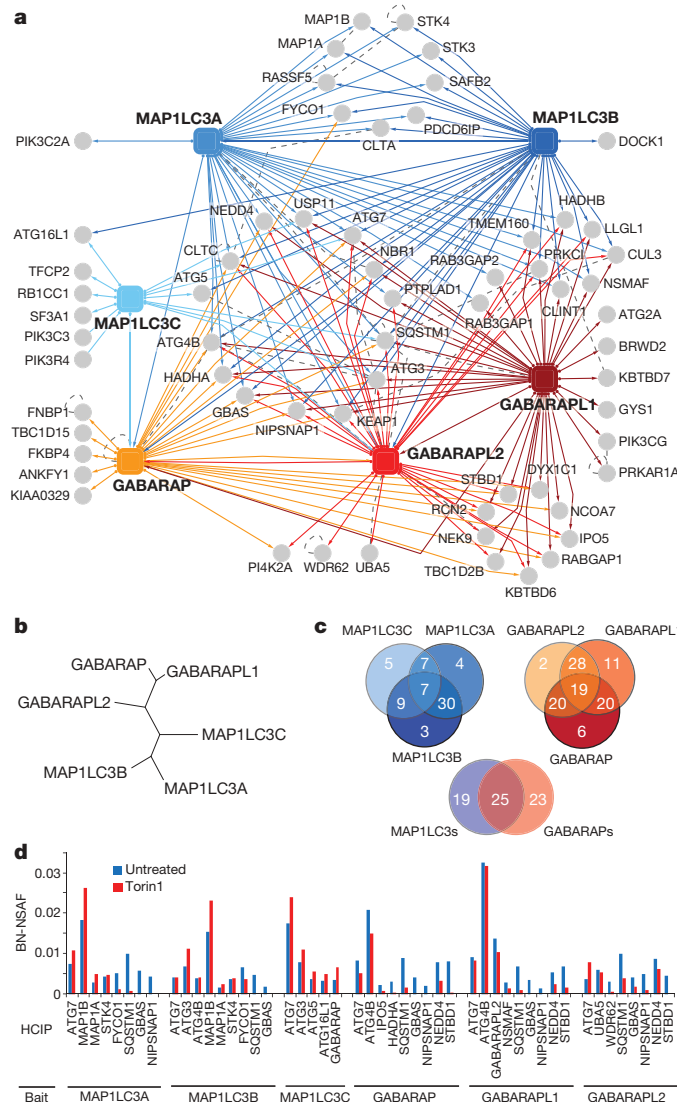


Figure 3 | The ATG8 subnetwork. **a**, Proteomic analysis of MAP1LC3 and GABARAP isoforms (filled squares). **b**, Human ATG8 protein phylogenetic tree. **c**, Overlap of interacting proteins found between and among MAP1LC3 and GABARAP subfamilies by LC-MS/MS. **d**, Effect of autophagy activation by Torin1 on HCIP-ATG8 association. BN-NSAF, bait normalized normalized spectral abundance factor.

found to interact with BECN1 and PIK3C3 (Fig. 2b), as recently reported^{13–15}. Cumulatively, 213 of 243 HCIPs in these 6 subnetworks are not present in BIOGRID or MINT databases. Moreover, 50% of the interactions tested (47 of 94) by LC-MS/MS were found reciprocally (Supplementary Fig. 6c).

Inhibition of mTOR promotes autophagosome formation, but it is unclear to what extent core interactions within the AIN are reorganized upon mTOR inhibition. In 293T cells used here, inhibition of mTOR using the small-molecule inhibitor Torin1 (200 nM) led to an increase in the extent of MAP1LC3-II (LC3-II) above the level found in untreated cells (basal conditions) (Supplementary Fig. 6g), signalling upregulation of the pathway. We performed proteomics on nine subunits of the conjugation, protein kinase, membrane recycling and membrane curvature complexes with and without a 6 h incubation of cells with Torin1. To quantify changes in subnetwork assembly, we used a previously described label-free semiquantitative LC-MS/MS approach (see Methods)¹⁶. Among the 44 HCIPs that passed the strict threshold necessary for quantification, 39 maintained interactions in the presence of Torin1 or increased (20–50%) (Fig. 2g). For example, enhanced association was seen between

components within ATG12–ATG5–ATG16L1 and PIK3C3–BECN1–UVRAG complexes (Fig. 2g). In contrast, association between ATG2A, ATG2B and WDR45 was unaltered by mTOR inhibition (Fig. 2g). Although further studies using more quantitative approaches are required to elucidate how activation of the pathway globally affects temporal assembly and disassembly of the AIN, these data indicate the absence of large-scale changes in core conjugation, lipid kinase and recycling complexes upon mTOR inhibition and imply the possible use of post-translational modification to induce pathway activation.

The ATG8 autophagy receptor subnetwork

Proteins of the UBL-containing ATG8 family are central coordinators of autophagosome assembly, maturation and lysosomal fusion^{1–3}. Upon C-terminal lipidation with PE by an ATG7–ATG3 activation and transfer cascade¹⁷, ATG8 is incorporated into the autophagosomal membrane where it promotes recruitment of cargo^{18,19}, and possibly regulatory factors. Recent work has revealed that cargo recruitment often involves the use of a conserved surface on ATG8 that we refer to as the LIR docking site (LDS); this LDS interacts with a conserved hydrophobic W/YXXL motif in cargo binding proteins referred to as the LC3-interaction region (LIR)²⁰ (Supplementary Fig. 11c). Mutations in LDS or LIR motifs reduce the binding of LIR-containing cargo adaptors such as NBR1, SQSTM1 (also called p62 or sequestosome) and NIX to ATG8 proteins, and disrupt transfer of cargo to the lysosome^{18–21}. NBR1 and SQSTM1 contain ubiquitin binding domains in addition to the LIR motif and have been implicated in recruitment of ubiquitinated cargo, whereas NIX recruits mitochondria²¹. Among the six ATG8 orthologues in mammals, MAP1LC3A, MAP1LC3B, MAP1LC3C and GABARAP are known to be conjugated to PE, incorporated into autophagosomes and interact with known cargo adaptors^{1–3,18–21}. Much less is known about the functions of GABARAPL1 (also called ATG8L) and GABARAPL2 (also called GATE-16), although the latter has been implicated in intra-Golgi vesicle transport³. Given that the high frequency of LIR motifs across the proteome makes the use of predictive approaches in the identification of ATG8-interacting proteins challenging, more direct approaches are required to identify regulatory and cargo adaptor proteins that function together with ATG8.

Through an analysis of the 6 human ATG8 proteins, we identified 67 HCIPs (Fig. 3a, b, Supplementary Fig. 8a and Supplementary Table 2), significantly expanding the number of candidate ATG8 interacting proteins. Included among these are known targets such as SQSTM1 and NBR1^{18,20}, as well as components of the conjugation apparatus (Fig. 3a). Fifty-two per cent of the GO process terms in this network are linked with vesicle transport, GTPase signalling, protein/amino acid modification, protein localization and transport, proteolysis, ubiquitin and phosphorylation ($P \approx 10^{-4}$ – 10^{-15}) (Supplementary Fig. 5a), and ATG8 interacting proteins are enriched in lipid kinase, WD40 and GTPase regulatory domains (TBC, NIPSNAP), among others ($P \approx 10^{-2}$ – 10^{-5}) (Supplementary Fig. 8b). Solely on the basis of LC-MS/MS data, we found that approximately one-third of interacting proteins were specific for the MAP1LC3 and GABARAP subfamilies, respectively, whereas one-third associated with both subfamilies (Fig. 3c). As described below, this may reflect the relative abundance and distribution of the various interacting proteins with ATG8 orthologues *in vivo*, rather than absolute specificity for a particular ATG8 orthologue.

We also examined the effect of pathway activation by means of mTOR inhibition on the ATG8 subnetwork (Fig. 3d and Supplementary Table 4). ATG7 and ATG4B maintained association with ATG8 family members 6 h after Torin1 treatment, whereas MAP1B displayed increased association with MAP1LC3A and MAP1LC3B. In contrast, several proteins including SQSTM1, GBAS (also called NIPSNAP2), NIPSNAP1 and NEDD4 displayed strongly reduced association with multiple ATG8 orthologues

(Fig. 3d). SQSTM1 is degraded upon autophagic delivery to the lysosome, potentially explaining the loss of SQSTM1 in these experiments and raising the possibility that other proteins with this behaviour are targeted for degradation in a similar manner.

In vitro ATG8 subnetwork validation

Reciprocal proteomic analysis revealed 40% validation (26 of 65) of interactions in the ATG8 network (Supplementary Fig. 8a). However, because the small size of ATG8 proteins (~ 14 kDa) limits the sensitivity in their detection by LC-MS/MS, we directly examined the interaction of GST–ATG8 proteins with 29 ATG8-interacting proteins synthesized *in vitro*. In total, 130 of the 145 interactions tested (90%) were confirmed (Fig. 4a and Supplementary Fig. 10a–c). Likewise, 85% of 115 interactions tested with 23 Myc-tagged ATG8-interacting proteins expressed in 293T cells were confirmed (Supplementary Fig. 9a–d). Of the proteins tested that were found only in association with the MAP1LC3 subnetwork by proteomics, all could associate with GABARAP proteins *in vitro* (Fig. 4a). Similarly, of the 15 proteins tested that were found only in association with the GABARAP subnetwork by proteomics, 12 and 14 were able to associate with MAP1LC3B and MAP1LC3C, respectively (Fig. 4a). Thus, specificity of ATG8 interacting proteins for MAP1LC3 and GABARAP subfamily members (Fig. 3d) may be more relaxed than appreciated by direct proteomic analysis *in vivo*, or alternatively, specificity may be controlled by cellular factors not present in the *in vitro* setting.

LIR-dependence of the ATG8 subnetwork

To examine the extent to which ATG8 binding proteins use an LIR–LDS interface, 34 ATG8-interacting proteins were tested for *in vitro* binding to GST-tagged GABARAP or MAP1LC3B in which the LDS was mutated (Y49A/L50A for GABARAP or F52A/L53A for MAP1LC3B) (Fig. 4b and Supplementary Fig. 11c)¹⁸. An additional mutant (R70A in MAP1LC3B and R67A in GABARAP) near the LDS was also tested (Supplementary Fig. 11a, b)¹⁸. In total, 60% (20 of 33) of GABARAP-interacting proteins displayed a reduction (20–90%) in binding with the LDS mutant when compared with wild-type GABARAP in parallel, whereas the R67A mutant had no effect on binding (Fig. 4b). Similarly, 38% (9 of 24) of MAP1LC3B-interacting proteins associated with GST–MAP1LC3B in an LDS-dependent manner (Fig. 4b). Eight proteins displayed loss of binding with both MAP1LC3B and GABARAP LDS mutants (Fig. 4b). Thus, a substantial fraction of the ATG8 subnetwork uses the LDS for assembly. In contrast with GABARAP, 18 proteins displayed reduced binding with the MAP1LC3B(R70A) mutant, indicating a specialized role for this residue (Supplementary Fig. 11b, d). These results indicate LDS-independent and -dependent mechanisms for ATG8 network assembly, and raise the possibility that a single ATG8 UBL fold may simultaneously associate with two or more interacting proteins to generate a signalling complex.

ATG8 lipidation and subnetwork assembly

The ATG8 C-terminal glycine is required for conjugation to PE, facilitating incorporation into autophagosomes³. To determine the extent to which formation of the ATG8 subnetwork depends upon the C-terminal glycine, we performed a comparative analysis of wild-type and ATG8(Δ Gly) proteins (GABARAP, GABARAPL1, GABARAPL2, MAP1LC3A and MAP1LC3B) (see Methods)¹⁶. Among the 28 HCIPs that passed the strict threshold required for quantification, 15 remained associated or increased association with ATG8(Δ Gly) (Fig. 4c, Supplementary Fig. 12 and Supplementary Table 3). In contrast, 13 proteins displayed reduced binding with one or more ATG8(Δ Gly) isoform. Most notable was the near complete loss of association with both ATG7 and ATG3 (Fig. 4c, Supplementary Fig. 12), revealing the importance of the C-terminal glycine and possibly thioester formation for tight association with the conjugation apparatus. Interestingly, association

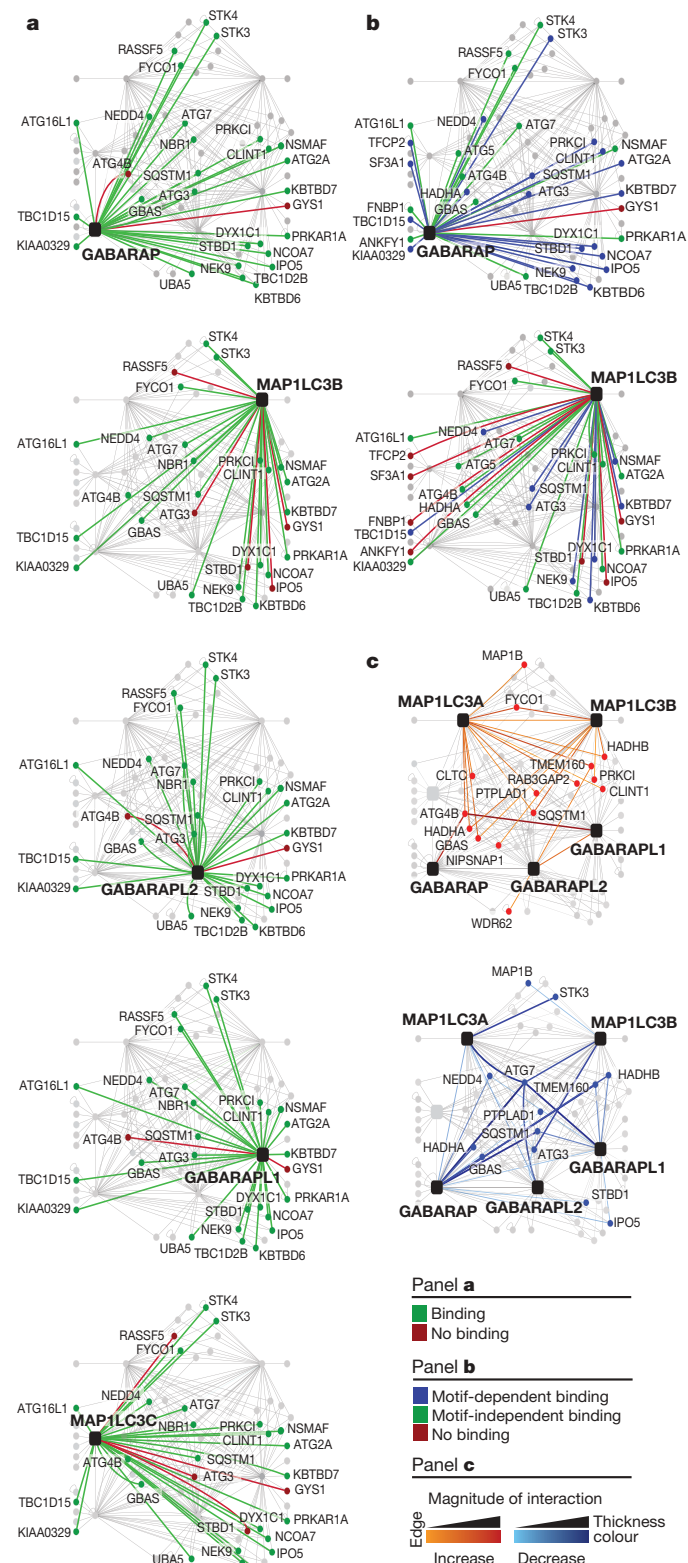
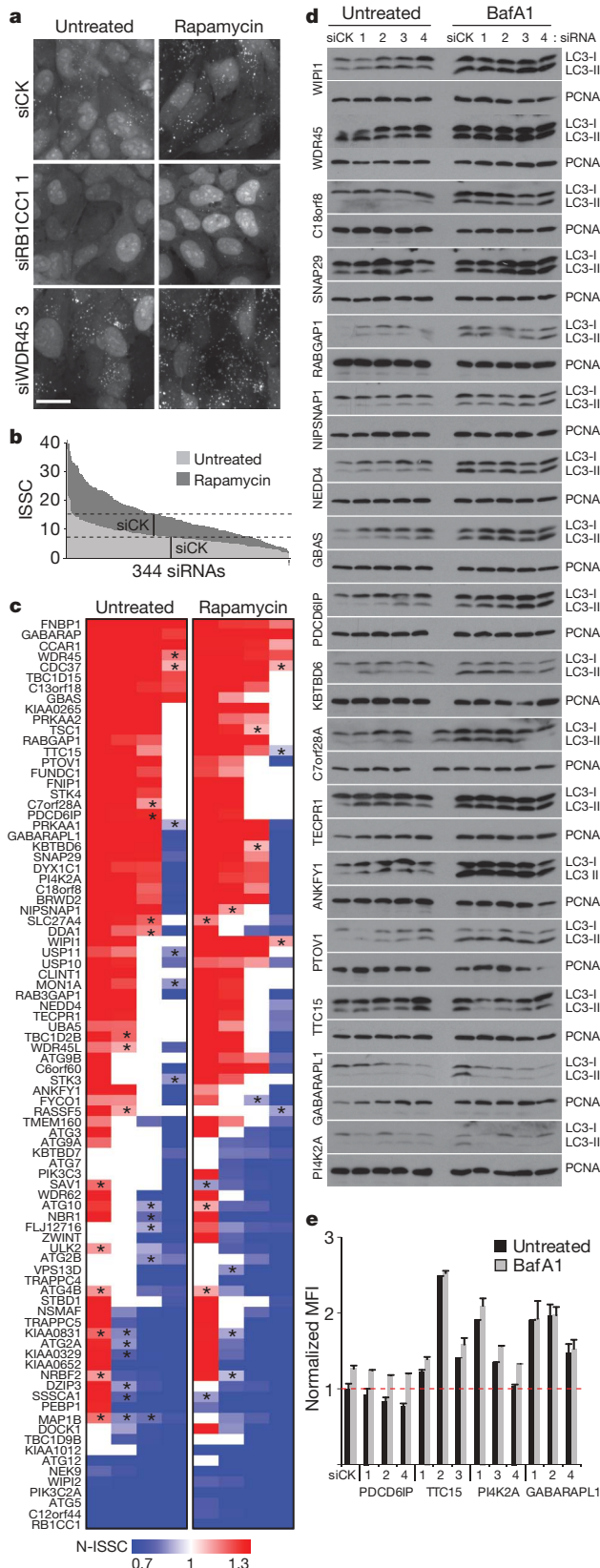


Figure 4 | Specificity within the ATG8 subnetwork. **a**, *In vitro* validation. S-tagged proteins were tested for GST–ATG8 binding (Supplementary Fig. 10). Green, binding; red, no binding. **b**, LDS dependence. As in panel **a** using wild-type, GABARAP(Y49A/L50A) or MAP1LC3B(F52A/L53A) proteins (Supplementary Fig. 11a, b). Blue edges, loss of binding; green edges, binding maintained; red edges, no binding with wild type. **c**, ATG8(Δ Gly) dependence. Wild-type and ATG8(Δ Gly) proteins from 293T cells were subjected to LC-MS/MS. Blue edge, decreased binding; red edge, increased binding. (See Supplementary Fig. 12a and Supplementary Table 3.)

**Figure 5 | RNAi analysis of the autophagy interaction network.**

a, GFP–MAP1LC3B foci after RNAi and/or rapamycin treatment in U2OS cells. Scale bar, 20 μ m. **b**, Integrated spot signal per cell (ISSC) for 344 siRNAs targeting 86 genes ($n = 4$). Control siRNA (siCK) is indicated by black vertical bars. **c**, Normalized ISSC (N-ISSC) for GFP–MAP1LC3B in U2OS cells with or without rapamycin (6 h) (4 siRNAs per gene with each bar representing one of four siRNAs). Unless noted otherwise, $P < 0.01$ using Students *t*-test; *, $P < 0.05$; white rectangles, $P > 0.05$. **d**, Anti-LC3 blots of U2OS cell extracts after depletion of the indicated proteins in the presence or absence of BafA1 (100 nM, 3 h), and re-probed with anti-PCNA. LC3-I and LC3-II represent unconjugated and PE-conjugated MAP1LC3 proteins, respectively. **e**, Normalized mean fluorescence intensity (MFI) of GFP–MAP1LC3B cells after depletion with the indicated siRNAs in the presence or absence of BafA1. Error bars indicate standard deviation; $n = 2$.

RNAi analysis of the AIN

Autophagosomes can be marked with GFP–MAP1LC3 and GFP–GABARAP (refs 1–3), and depletion of positive (for example, PIK3C3) or negative (for example, RUBICON) regulators decreases or increases the number of autophagosomes, respectively¹³. We initially examined whether depletion of 86 genes in the AIN using RNA interference (RNAi) (4 short interfering RNAs (siRNAs) per gene in quadruplicate) altered basal or rapamycin-stimulated autophagosome production in U2OS cells expressing GFP–MAP1LC3B. To quantify autophagosome production, we used an algorithm that determines cytoplasmic integrated spot signal per cell (ISSC) over 400 ± 100 cells (Fig. 5a–c). The ISSC provides a measure of both the number and intensity of autophagosomes integrated across the cell cytoplasm (see Methods). Under these conditions, rapamycin induced a ~2.5-fold increase in ISSC in cells transfected with a control siRNA (siCK) (Fig. 5a, b and Supplementary Fig. 13b). A cross-section of genes in the AIN was examined, including known autophagy proteins used as controls, but we focused primarily on proteins with multiple interactions within the network, and proteins whose domains or GO process identifiers potentially linked them to the autophagy process.

As expected, depletion of ATG5, ATG12, RB1CC1, C12orf44 (ATG101) and KIAA0652 (ATG13) revealed a significant reduction in normalized ISSC (N-ISSC) under either basal or induced conditions (Fig. 5a, c). Depletion of 31 genes with 2 or more siRNAs resulted in a reduction in autophagosomes, and this was increased to 38 genes in the presence of rapamycin (Fig. 5c, Supplementary Table 6 and Supplementary Fig. 13g, h). Among the positive regulators of autophagosome formation were the protein kinase NEK9, the lipid kinase PIK3C2A and the GTPase regulator TBC1D9B, each scoring with 3 or 4 independent siRNAs. The increase in the number of genes scoring in the presence of rapamycin may reflect a more stringent requirement for these genes when the pathway is induced. In contrast, depletion of 30 genes with 3 or 4 siRNAs led to increased autophagosomes under uninduced conditions and 25 genes in the presence of rapamycin (Fig. 5c and Supplementary Table 6), including WDR45, the BECN1 interacting protein C13orf18 and GBAS (Fig. 5c). Analogous studies in the context of GFP–GABARAP produced broadly similar results, indicating that a subset of the genes identified also control the formation of GFP–GABARAP-labelled vesicles (Supplementary Fig. 13d–f). Overall, there was strong correspondence (75%) between the extent of depletion by quantitative PCR or protein abundance and N-ISSC (see Methods and Supplementary Fig. 13g, h).

Increased autophagosome number could reflect either an increase in the production of autophagosomes (for example, depletion of a negative regulator of an early step in the pathway) or inhibition of later steps in the pathway such as fusion with the lysosome. To examine this question, we used established autophagosomal flux assays^{22,23} that examine the steady-state level of MAP1LC3–PE (LC3-II) in the presence and absence of bafilomycin A1 (BafA1, an inhibitor of autophagosome–lysosome fusion) (see Methods). Proteins for which depletion leads to an increase in the steady-state

with some proteins (for example, SQSTM1) was maintained with MAP1LC3(ΔGly) proteins but was lost with GABARAP(ΔGly) proteins (Fig. 4c), raising the possibility that the two ATG8 subfamilies have distinct lipidation requirements for assembly with particular binding partners. These data indicate that a cohort of ATG8 subnetwork proteins may assemble before ATG lipidation or independent of incorporation of ATG8–PE into the autophagosome.

abundance of LC3-II upon BafA1 treatment are considered to cause upregulation of the pathway, whereas proteins for which depletion has no effect on steady-state LC3-II levels upon BafA1 addition are considered to be required for flux through the pathway^{22,23}. We tested 17 genes for which depletion led to increased N-ISSC using RNAi (Fig. 5d). In 14 cases, addition of BafA1 led to an increase in the steady-state abundance of LC3-II relative to PCNA used as a loading control, indicating that depletion of these genes upregulates the autophagy system. In contrast, LC3-II levels in cells depleted of TTC15, GABARAPL1 and PI4K2A were not further increased upon BafA1 treatment (Fig. 5d). Thus, these genes seem to block flux through the pathway. These results were confirmed using an independent flow-cytometry assay (Fig. 5e and Supplementary Fig. 13i; see Methods). The normalized mean fluorescence intensity (MFI) of GFP-MAP1LC3B cells depleted of PCDC6IP was increased upon BafA1 treatment, as expected based on LC3 immunoblotting; however, cells depleted of GABARAPL1, TTC15 and PI4K2A displayed an increase in the normalized MFI that did not increase further upon BafA1 treatment (Fig. 5e). Thus, genes identified in the AIN seem to function at distinct stages in the autophagy process based on these flux assays. Further studies are required to pinpoint steps in the process in which genes in the AIN function.

Discussion

As with any screening approach, the results reported here will require additional validation using more directed experiments. Most of the interactions identified here represent the network under ongoing

(basal) autophagy in cultured cells, and it is likely that components within the network will be enriched or released upon blockade or activation of the pathway. Indeed, our proteomic analysis of 15 pathway components revealed both gain and loss of components upon stimulation of autophagy by mTOR inhibition. Additional studies are required to elucidate fully and quantify the dynamics and importance of reorganization of the network upon pathway activation by various autophagic stimuli, and to identify mechanisms of action of genes for which depletion alters autophagosome formation in our RNAi experiments. Nevertheless, several potential functional links are suggested by analysis of proteins identified within the existing network. One surprising feature of the network is the extent of connectivity between the various signalling modules. In total, 22 cross-module links were found and each of the major subnetworks devoted to signalling (ULK1-RB1CC1, PIK3C3) and vesicle assembly (ATG2A) make interactions with ATG8 family members (Figs 1 and 6), indicating that ATG8 proteins may serve to organize regulatory functions during autophagosome formation. In addition, we identified a large cohort of proteins that associate with ATG8 orthologues, which may facilitate an understanding of the diversity of the human ATG8 proteins. The substantial overlap in binding partners for MAP1LC3 and GABARAP subfamilies (Figs 3 and 4) suggests that they have at least partially redundant roles in autophagy. ATG8-associated proteins could function as receptors that facilitate the engulfment of organelles and cellular proteins into the autophagosome, as is envisioned for NIX, NBR1 and SQSTM1 (refs 18, 21), or alternatively, could be regulators of the process. ATG8-associated

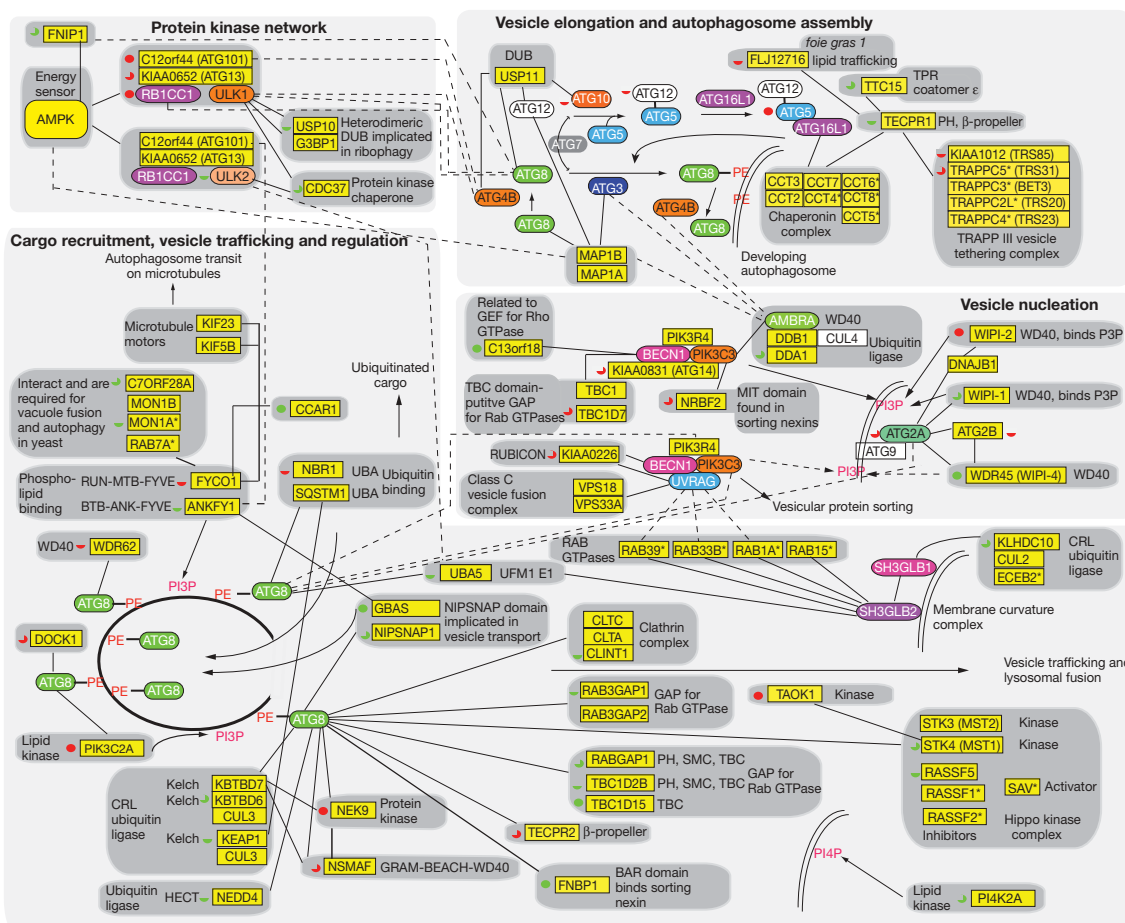


Figure 6 | Functional integration of the autophagy interaction network. Proteins in yellow boxes are HCIPs and proteins labelled with an asterisk were subthreshold (WD^N -score < 1.0) for HCIP identification. Dotted lines, cross-module interaction; solid lines, this study; dotted arrows, potential functional interactions. Red or green full circle, three-quarter circle and

half-circle represent a reduction or increase in autophagosomes with 4, 3 and 2 siRNAs, respectively, in GFP-MAP1LC3B-expressing U2OS cells without rapamycin. Proteins in white boxes were not found by proteomics. The six ATG8 family members are represented by ATG8.

proteins could also be targeted for degradation directly, as seems to be the case for SQSTM1 and NBR1 (ref. 18). Like MAP1LC3 and GABARAP, we found that GABARAPL1 and GABARAPL2 also associated with ATG7, ATG3 and ATG5, indicating that these poorly understood ATG8 family members are also under the control of the PE conjugation system.

Multiple proteins in the ATG8 network (Fig. 6) contain related domains frequently implicated in vesicle function, including: (1) GBAS (NIPSNAP2) and NIPSNAP1 containing the NIPSNAP domain implicated in vesicle transport/fusion; (2) RABGAP, RAB3GAP1, RAB3GAP2, TBC1D2B and TBC1D15 which contain putative RAB GTPase activating functions; and (3) phosphatidylinositol 3-phosphate (PI3P)-binding FYVE domain-containing proteins FYCO1 and ANKFY1. FYCO1 was independently identified as a Rab7 effector and an ATG8 binding protein, and found to associate with the exterior of autophagosomes via its FYVE domain²⁴, as we have also found (data not shown). Depletion of FYCO1 led to perinuclear accumulation of residual autophagosomes, and a role for FYCO1 in tethering autophagosomes to plus-end-directed microtubule motor proteins was proposed to explain this phenotype²⁴. We found that FYCO1 associates with two microtubule motor proteins—kinesin (KIF) 5B and KIF23 (Fig. 6 and Supplementary Fig. 6e). Interestingly, depletion of KIF5B leads to perinuclear accumulation of autophagosomes²⁵, allowing us to propose that KIF5B links FYCO1-positive autophagosomes to microtubules to maintain cortical localization. We also identified C7orf28A and MON1B, as well as MON1A and RAB7A with subthreshold WD^N-scores, in association with FYCO1 (Fig. 6). MON1 is orthologous to Mon1p, which in yeast is required for vacuole fusion and autophagy, and interacts with Ccz1p, the RAB7 orthologue Ypt7p, and the vacuole *cis*-SNARE complex²⁶. Although we were unable to find human orthologues of Ccz1p by conventional sequence searches, C7orf28A and Ccz1p share a distantly related domain of unknown function (DUF1712 in PFAM), indicating that C7orf28A and Ccz1p are functional orthologues. C7orf28A depletion led to an increase in autophagosome number without blocking autophagosomal flux (Fig. 5d). Thus, FYCO1 seems to function as a platform for assembly of vesicle fusion and trafficking factors. Interestingly, a requirement for orthologues of Mon1p and Ccz1p in apoptotic cell phagocytosis in *Caenorhabditis elegans* was recently demonstrated²⁷. ANKFY1 associates with both PI3P and RAB5 on endosomes and stimulates endosomal fusion²⁸, and depletion of ANKFY1 also leads to increased autophagosomal number without blocking flux (Fig. 5d). The interaction of ATG8 proteins with multiple RAB GTPase regulatory proteins suggests a role for ATG8 in controlling localized RAB activation and vesicle dynamics.

Protein kinases feature prominently in the AIN (Fig. 6). Consistent with recent studies, we found that both ULK1 and ULK2 associate with the RB1CC1–ATG13–C12orf44 (ATG101) regulatory complex (Fig. 2d), which is under the control of mTOR⁵. We also found that depletion of ULK2, like depletion of RB1CC1, leads to a reduction in autophagosome formation (Fig. 5c)²⁹. Consistent with a common pathway for assembly, both ULK1 and ULK2 associated with the CDC37 subunit of the HSP90 chaperone complex implicated in stabilization of a substantial fraction of the kinome³⁰. In yeast and *Drosophila*, AMPK is required for autophagy, but its target(s) in the pathway remain unknown. Interestingly, we found that both ULK1 and ULK2 associate with AMPK (Fig. 2), providing the first biochemical link between these kinases and the cell's energy sensing system. Additionally, our proteomic analysis of the AMPK complex revealed several known and candidate AMPK targets, including FNIP1, which was also found in association with GABARAP (Supplementary Tables 2 and 3). Further studies are required to elucidate any regulatory links between AMPK, ATG8 family members, and the ULK1/ULK2 complexes. Additional kinase complexes are linked with the cargo recruitment, vesicle trafficking and regulation subnetwork (Fig. 6), including NEK9 and components of

the Hippo kinase complex—STK3 (also called MST2) and STK4 (MST1)—implicated in cell growth control. STK4 and NEK9 have opposing roles in autophagosome formation, as measured by our RNAi screen (Fig. 5), and seem to bind ATG8 through distinct surfaces (Fig. 4b).

New components of the ATG8 conjugation, vesicle elongation and autophagosome assembly subnetwork were identified, including the previously unstudied TECPR1 protein, which interacts with the ATG12–ATG5–ATG16 complex (Figs 2a and 6), and a related protein, TECPR2, which was found in association with ATG8 orthologues (Fig. 6). TECPR1 also associated with FLJ12716, TTC15 and components of the TRAPP vesicle-tethering complex, including KIAA1012 (also known as TRS85), as well as TRAPPC2L (TRS20), TRAPPC3 (BET3), TRAPPC4 (TRS23) and TRAPPC5 (TRS31) with subthreshold WD^N-scores (Fig. 6 and Supplementary Table 2). In yeast, Trs85p has been shown to associate specifically with a unique form of the TRAPP complex, TRAPPIII (containing Trs20p, Trs23p, Trs31p, Bet3p, Bet5p, and Trs33p), is required for assembly of Atg8p onto pre-autophagosomal structures, and serves as a guanine nucleotide exchange factor for the GTPase Ypt1p³¹. We found that depletion of TRAPPC5, KIAA1012 (TRS85) and FLJ12716 (the human orthologue of the zebrafish *foie gras* (*fgr*; also called *foigr*) gene, mutation of which leads to defects in lipid trafficking in hepatocytes³²) led to a reduction in autophagosome formation (Fig. 5c). In contrast, depletion of TECPR1 and its associated protein TTC15 led to an increase in autophagosome number (Figs 5 and 6). Interestingly, depletion of TTC15 also resulted in a defect in flux, whereas depletion of TECPR1 did not, indicating that these proteins act at distinct steps in the process.

In yeast, Atg18p binds PI3P via its WD40 propeller, thereby directing the Atg18p–Atg2p complex to autophagosomal membranes. In mammalian cells, the Atg18p-related WIPI1 protein binds PI3P and associates with MAP1LC3-positive structures, but has not been reported to associate with either of the Atg2p orthologues (ATG2A and ATG2B)³³. ATG2A was detected in WIPI1 immune complexes. However, although we did not detect WIPI1 in ATG2A complexes, a previously unstudied WD40 protein, WDR45 (WIPI4), reciprocally bound ATG2A and also associated with ATG2B. WDR45 is phylogenetically related to both Atg18p and Atg21p (Supplementary Fig. 11e). Interestingly, ATG2A associated with ATG2B, suggesting that these two related proteins functionally interact (Fig. 2e). WIPI2, the putative orthologue of Atg21p, associated with ATG2A indirectly through DNAJB1 (Fig. 2e). Depletion of WDR45 or WIPI1 led to increased autophagosome number without blocking flux (Fig. 5d), whereas depletion of WIPI2 led to reduced autophagosome number (Fig. 5c), indicating distinct roles for WIPI proteins in the autophagy process. It remains to be determined whether WDR45 (WIPI4) also binds PI3P, and whether it functions in a manner analogous to Atg18p in yeast, possibly in combination with WIPI1.

Finally, several components of the ubiquitin-proteasome system are present in the AIN, including AMBRA1 (DCAF3), which we previously identified as a putative substrate adaptor for the CUL4–DDB1–DDA1 ubiquitin ligase³⁴ (Fig. 2b and Supplementary Fig. 6). The association of CUL4–DDB1–DDA1^{AMBRA1} with the PIK3C3–BECN1 complex⁶ suggests a role for ubiquitin-dependent proteolysis in the function or regulation of this complex. Two additional cullin-related ubiquitin ligases are also found in the AIN: the CUL2–ELOB–ELOC^{KLHD10} complex associated with the SH3GLB1 network (Fig. 2c), and the CUL3^{KBTBD6–KBTBD7} complex found associated with the GABARAP network (Fig. 3a and Supplementary Fig. 6). Moreover, the HECT E3 NEDD4 associates with multiple ATG8 proteins and has been previously linked with endosomal protein degradation³⁵. KBTBD6/KBTBD7 and NEDD4 associate with ATG8 in an LDS-independent manner and NEDD4 association decreases upon loss of the ATG8 C-terminal glycine, indicating a role for lipidation in NEDD4 assembly. Enzymes that remove ubiquitin from proteins also figure prominently in the AIN. For example, the ubiquitin-specific protease USP10

and its adaptor protein G3BP1 (ref. 9) were found to associate with the ULK1 complex and depletion of USP10 led to an increase in autophagosome number (Fig. 5c). Yeast orthologues of USP10 and G3BP1—Ubp3p and Bre5p—have been implicated in ribophagy³⁶. Further studies are required to determine whether ULK1 regulates USP10/G3BP1 function or vice versa.

These studies provide an insight into the organization of the mammalian autophagy interaction landscape and will serve as a resource for further mechanistic analysis of this pathway so critical for protein homeostasis.

METHODS SUMMARY

Proteins (Supplementary Table 1) were expressed in 293 (or 293T) cells and purified using anti-HA before proteomic analysis using CompPASS⁹. Proteomic data in searchable and downloadable formats are available at <http://pathology.hms.harvard.edu/labs/harper>Welcome.html>. For *in vitro* binding, GST–ATG8 proteins (2 µg) were incubated with ³⁵S-methionine-labelled interacting protein (3 µl) in 1 ml of lysis buffer. Proteins were subjected to SDS–PAGE and autoradiography. To measure autophagosome formation, U2OS cells expressing GFP–MAPILC3B or GFP–GABARAP were transfected in quadruplicate with 30 nM of the indicated siRNAs (Supplementary Table 5) using RNAiMax (Invitrogen). After 72 h with or without a 6 h treatment with rapamycin (200 nM), nuclei were stained with DRAQ5 and GFP-positive foci in 400 ± 100 cells quantified using an Opera high-throughput confocal microscope (Evotec) and an Acapella algorithm that measures integrated spot signal per cell cytoplasm, normalizing to a control siRNA (siCK) (Supplementary Table 6). Students *t*-test was used to determine statistical significance.

Full Methods and any associated references are available in the online version of the paper at www.nature.com/nature.

Received 13 January; accepted 25 May 2010.

Published online 20 June 2010.

1. Mizushima, N., Levine, B., Cuervo, A. M. & Klionsky, D. J. Autophagy fights disease through cellular self-digestion. *Nature* **451**, 1069–1075 (2008).
2. Levine, B. & Kroemer, G. Autophagy in the pathogenesis of disease. *Cell* **132**, 27–42 (2008).
3. Nakatogawa, H., Suzuki, K., Kamada, Y. & Ohsumi, Y. Dynamics and diversity in autophagy mechanisms: lessons from yeast. *Nature Rev. Mol. Cell Biol.* **10**, 458–467 (2009).
4. Kabeya, Y. et al. Atg17 functions in cooperation with Atg1 and Atg13 in yeast autophagy. *Mol. Biol. Cell* **16**, 2544–2553 (2005).
5. Mizushima, N. The role of the Atg1/ULK1 complex in autophagy regulation. *Curr. Opin. Cell Biol.* **22**, 132–139 (2010).
6. Simonsen, A. & Tooze, S. A. Coordination of membrane events during autophagy by multiple class III PI3-kinase complexes. *J. Cell Biol.* **186**, 773–782 (2009).
7. Hanada, T. et al. The Atg12–Atg5 conjugate has a novel E3-like activity for protein lipidation in autophagy. *J. Biol. Chem.* **282**, 37298–37302 (2007).
8. Legakis, J. E., Yen, W. L. & Klionsky, D. J. A cyclin protein complex required for selective autophagy. *Autophagy* **3**, 422–432 (2007).
9. Sowa, M. E., Bennett, E. J., Gygi, S. P. & Harper, J. W. Defining the human deubiquitinating enzyme interaction landscape. *Cell* **138**, 389–403 (2009).
10. Spiess, C., Meyer, A. S., Reissmann, S. & Frydman, J. Mechanism of the eukaryotic chaperonin: protein folding in the chamber of secrets. *Trends Cell Biol.* **14**, 598–604 (2004).
11. Wang, Z., Wilson, W. A., Fujino, M. A. & Roach, P. J. Antagonistic controls of autophagy and glycogen accumulation by Snf1p, the yeast homolog of AMP-activated protein kinase, and the cyclin-dependent kinase Pho85p. *Mol. Cell. Biol.* **21**, 5742–5752 (2001).
12. Lippai, M. et al. SNF4Aγ, the *Drosophila* AMPK γ subunit is required for regulation of developmental and stress-induced autophagy. *Autophagy* **4**, 476–486 (2008).
13. Matsunaga, K. et al. Two Beclin 1-binding proteins, Atg14L and Rubicon, reciprocally regulate autophagy at different stages. *Nature Cell Biol.* **11**, 385–396 (2009).
14. Zhong, Y. et al. Distinct regulation of autophagic activity by Atg14L and Rubicon associated with Beclin 1-phosphatidylinositol-3-kinase complex. *Nature Cell Biol.* **11**, 468–476 (2009).

15. Itakura, E., Kishi, C., Inoue, K. & Mizushima, N. Beclin 1 forms two distinct phosphatidylinositol 3-kinase complexes with mammalian Atg14 and UVrag. *Mol. Biol. Cell* **19**, 5360–5372 (2008).
16. Sardiu, M. E. et al. Probabilistic assembly of human protein interaction networks from label-free quantitative proteomics. *Proc. Natl. Acad. Sci. USA* **105**, 1454–1459 (2008).
17. Schulman, B. A. & Harper, J. W. Ubiquitin-like protein activation: the apex for diverse signaling pathways. *Nature Rev. Mol. Cell Biol.* **10**, 319–331 (2009).
18. Kirkin, V. et al. A role for NBR1 in autophagosomal degradation of ubiquitinated substrates. *Mol. Cell* **33**, 505–516 (2009).
19. Kirkin, V., McEwan, D. G., Novak, I. & Dikic, I. A role for ubiquitin in selective autophagy. *Mol. Cell* **34**, 259–269 (2009).
20. Noda, N. N. et al. Structural basis of target recognition by Atg8/LC3 during selective autophagy. *Genes Cells* **13**, 1211–1218 (2008).
21. Novak, I. et al. Nix is a selective autophagy receptor for mitochondrial clearance. *EMBO Rep.* **11**, 45–51 (2009).
22. Mizushima, N., Yoshimori, T. & Levine, B. Methods in mammalian autophagy research. *Cell* **140**, 313–326 (2010).
23. Mizushima, N. & Yoshimori, T. How to interpret LC3 immunoblotting. *Autophagy* **3**, 542–545 (2007).
24. Pankiv, S. et al. FYCO1 is a Rab7 effector that binds to LC3 and PI3P to mediate microtubule plus end-directed vesicle transport. *J. Cell Biol.* **188**, 253–269 (2010).
25. Cardoso, C. M. et al. Depletion of kinesin 5B affects lysosomal distribution and stability and induces peri-nuclear accumulation of autophagosomes in cancer cells. *PLoS ONE* **4**, e4424 (2009).
26. Wang, C. W., Stromhaug, P. E., Kauffman, E. J., Weisman, L. S. & Klionsky, D. J. Yeast homotypic vacuole fusion requires the Ccz1-Mon1 complex during the tethering/docking stage. *J. Cell Biol.* **163**, 973–985 (2003).
27. Kinchen, J. M. & Ravichandran, K. S. Identification of two evolutionarily conserved genes regulating processing of engulfed apoptotic cells. *Nature* **464**, 778–782 (2010).
28. Schnatwinkel, C. et al. The Rab5 effector Rabankyrin-5 regulates and coordinates different endocytic mechanisms. *PLoS Biol.* **2**, e261 (2004).
29. Jung, C. H. et al. ULK-Atg13-FIP200 complexes mediate mTOR signaling to the autophagy machinery. *Mol. Biol. Cell* **20**, 1992–2003 (2009).
30. Karnitz, L. M. & Felts, S. J. Cdc37 regulation of the kinome: when to hold 'em and when to fold 'em. *Sci. STKE* **2007**, pe22 (2007).
31. Lynch-Day, M. A. et al. Trs85 directs a Ypt1 GEF, TRAPPIII, to the phagophore to promote autophagy. *Proc. Natl. Acad. Sci. USA* **107**, 7811–7816 (2010).
32. Sadler, K. C., Amsterdam, A., Soroka, C., Boyer, J. & Hopkins, N. A genetic screen in zebrafish identifies the mutants *vps18*, *nf2* and *foie gras* as models of liver disease. *Development* **132**, 3561–3572 (2005).
33. Jeffries, T. R., Dove, S. K., Michell, R. H. & Parker, P. J. PtdIns-specific MPR pathway association of a novel WD40 repeat protein, WIP149. *Mol. Biol. Cell* **15**, 2652–2663 (2004).
34. Jin, J., Arias, E. E., Chen, J., Harper, J. W. & Walter, J. C. A family of diverse Cul4-Ddb1-interacting proteins includes Cdt2, which is required for S phase destruction of the replication factor Cdt1. *Mol. Cell* **23**, 709–721 (2006).
35. Sakata, T. et al. *Drosophila* Nedd4 regulates endocytosis of notch and suppresses its ligand-independent activation. *Curr. Biol.* **14**, 2228–2236 (2004).
36. Kraft, C., Deplazes, A., Sohrmann, M. & Peter, M. Mature ribosomes are selectively degraded upon starvation by an autophagy pathway requiring the Ubp3p/Bre5p ubiquitin protease. *Nature Cell Biol.* **10**, 602–610 (2008).

Supplementary Information is linked to the online version of the paper at www.nature.com/nature.

Acknowledgements We thank I. Dikic for discussions and for sharing unpublished data, D. Bowman and J. Ringeling for assistance with Acapela software, N. Perrimon, S. Mohr and M. Ocana for access to the Opera microscope, and N. Gray for Torin1. This work was supported by grants to J.W.H. from Millennium Pharmaceuticals, the National Institutes of Health, and the Paul F. Glenn Foundation on Aging. C.B. is a Humboldt Postdoctoral Fellow.

Author Contributions C.B. and M.E.S. performed experiments, analysed data and co-wrote the paper. S.P.G. provided proteomic infrastructure support and interpreted data. J.W.H. directed the research, interpreted data and wrote the paper.

Author Information Reprints and permissions information is available at www.nature.com/reprints. The authors declare competing financial interests: details accompany the full-text HTML version of the paper at www.nature.com/nature. Readers are welcome to comment on the online version of this article at www.nature.com/nature. Correspondence and requests for materials should be addressed to J.W.H. (wade_harper@hms.harvard.edu).

METHODS

Plasmids and cell lines. Sequence-verified ORF clones (Supplementary Table 1) in pDONR223 were recombined into either the Gateway destination vector MSCV-N-Flag-HA-IRES-PURO (LTR-driven expression) or pHAGE-N-Flag-HA (lentiviral vector) using λ recombinase⁹. After packaging in 293T cells, viruses were used to infect the indicated cell lines and selection accomplished using 1 $\mu\text{g ml}^{-1}$ puramycin. The pHAGE-N-Flag-HA vector was used in transient transfections (293T cells, Lipofectamine 2000 (Invitrogen)) for a subset of AIN proteins that were toxic when expressed constitutively from the LTR promoter (Supplementary Table 1).

Protein purification. For standard purifications, cells from four 15-cm tissue culture dishes at ~80% confluence (~10⁷ cells) were lysed in a total volume of 4 ml of lysis buffer (50 mM Tris-HCl pH 7.5, 150 mM NaCl, 0.5% Nonidet P40, Roche complete EDTA-free protease inhibitor cocktail) for 1 h with gentle rocking at 4 °C. In some experiments, cells were incubated with 200 nM Torin1³⁷ (a gift from N. Gray) for 6 h before harvesting. Lysates were cleared using centrifugation (13,000 r.p.m., 10 min), the supernatant was filtered through 0.45 μm spin filters (Millipore) to further remove cell debris, and the resulting material subjected to immunoprecipitation with 60 μl of immobilized anti-HA (Sigma) resin (50% slurry) at 4 °C with gentle inversion. Resin containing immune complexes was washed with 1 ml ice-cold lysis buffer 5 times followed by five 1-ml phosphate-buffered saline washes. Proteins were eluted with three 50 μl incubations with 250 $\mu\text{g ml}^{-1}$ HA-peptide (Sigma) in PBS for 30 min each at 22 °C, and elutions were pooled for a final volume of 150 μl . Proteins in each elution were precipitated with 20% trichloroacetic acid (TCA) and the resulting pellet washed once with 10% TCA and four times with cold acetone.

Mass spectrometry. TCA-precipitated proteins were re-suspended in 30 μl 100 mM ammonium bicarbonate pH 8.0 with 10% acetonitrile and sequencing grade trypsin (750 ng, Promega) and incubated at 37 °C for 4 h. Digested samples were then loaded onto stage tips and washed as described previously⁹. Peptides were eluted with 50% acetonitrile, 5% formic acid, dried, and re-suspended in 10 μl of 5% acetonitrile, 5% formic acid. For each LC-MS/MS run using an LTQ linear ion trap mass spectrometer (ThermoFinnigan), 4 μl was loaded onto an 18 cm × 125 μm (ID) C18 column and peptides eluted using a 50 min 8–26% acetonitrile gradient. Spectra were acquired using a Top-10 method. Each sample was shot twice in succession, followed by a wash with 70% acetonitrile, 30% isopropanol. The resulting spectra were searched using Sequest against a target-decoy database of human tryptic peptides. The resulting list of identifications for each was loaded into CompPASS for further processing and analysis⁹. All of the proteomic data from this work can be obtained at <http://pathology.hms.harvard.edu/labs/harper/Welcome.html>.

Validation of protein interactions. For reciprocal tagging MS validation, HCIPs were tagged, expressed and purified using the same methodology as used for the primary baits. For western analysis, the ORF for the HCIP of interest was recombined into pDEST-CMV-N-Myc using Gateway cloning methods and transfected into 293T cells using Lipofectamine 2000 (Invitrogen). After 48 h, whole-cell extracts were incubated with the indicated GST-ATG8 protein (2 μg per 10 μl resin) purified from bacteria. Washed beads were subjected to SDS-PAGE and immunoblotting using anti-Myc antibodies. For GST pull down with *in vitro* expressed ³⁵S-labelled proteins, ORFs of interest were recombined into pET-56-DEST (Novagen) as described above and co-transcribed/translated in the TNT T7 coupled reticulocyte lysate system (Promega). The indicated GST-ATG8 orthologue (or GST as a control) was expressed in *Escherichia coli* (BL21) cells and purified using GSH-Sepharose. GST fusion proteins (2 μg in 10 μl of resin) were incubated with 3 μl of *in vitro* translated and ³⁵S-methionine-labelled interacting protein in a total volume of 1 ml of 25 mM Tris-HCl, 0.5% NP40, 150 mM NaCl, 6 mM EDTA (lysis buffer). After 1 h, the resin was washed 5 times with 1 ml of lysis buffer, bound proteins subjected to SDS-PAGE, Coomassie staining and autoradiography.

High-throughput autophagosome assays. To develop a 384-well plate based microscopic assay that measures autophagosome formation, we created clonal U2OS cells that stably expressed either GFP-MAP1LC3B or GFP-GABARAP via a lentivirus. These cells were reverse transfected in quadruplicate with 30 nM of the indicated siRNAs (Supplementary Table 5) using RNAiMAX (Invitrogen) and after 72 h with or without a 6 h treatment with rapamycin (200 nM), nuclei were stained with DRAQ5 (Cell Signaling) and GFP-positive foci quantified using an Opera high-throughput confocal microscope (Evotec) in the *Drosophila* RNAi Screening Center (DRSC) at Harvard Medical School. As a control siRNA and for normalization purposes, we used siCK (GAUCCGCAGCGACAUCAACCUGA) (Supplementary Table 5). This siRNA lacks complementarity with any mRNA in the human and mouse genome and gives an indistinguishable number of autophagosomes when compared with mock-transfected cells (data not shown). We imaged five planes at ten positions in each well of the plate with a $\times 40$ lens and then performed image analysis on 400 ± 100 cells using custom scripts in Acapella software (Evotec) that determine the maximum intensity projection, identify nucleus and cytoplasm, and individual spots, and then outputs the number of spots

(GFP-MAP1LC3B or GFP-GABARAP foci) per cell cytoplasm and the integrated spot signal per cell cytoplasm. The results of quadruplicate assays were averaged before determination of the standard deviation and the normalized average spot signal per cell across multiple plates (Supplementary Table 6). Students *t*-test was used to determine statistical significance.

Autophagic flux was measured in live cells using a previously described flow cytometric analysis³⁸ and by immunoblotting of LC3²². For flow cytometry, U2OS cells expressing GFP-MAP1LC3B in 96-well format were reverse transfected with siRNAs (20 nM) in duplicate and after 72 h, cells were treated with BafA1 (3 h, 100 nM). A total of 10,000 cells was analysed for GFP by flow cytometry and analysed using FLOWJO. For LC3-II immunoblotting assays, cells were transfected with siRNAs and after 72 h, cells were either left untreated or treated with BafA1 (3 h, 100 nM) before lysis in 50 mM Tris (pH 7.5) buffer containing 150 mM NaCl, 0.1% SDS, 1% Nonidet-P40, and 0.5% deoxycholate. Blots were probed with anti-LC3 (Cell Signaling Technologies) and re-probed with anti-PCNA (Santa Cruz Biotechnology) as a loading control.

Quantitative RT-PCR. U2OS cells were reverse transfected in triplicate with RNAiMAX (Invitrogen) and 30 nM siRNA oligo (Supplementary Table 5). Total RNA was extracted from each sample 72 h after transfection using Trizol reagent (Invitrogen). cDNA was then prepared from ~1 μg of total RNA using the Superscript II First-Strand Synthesis kit (Invitrogen). Quantitative RT-PCR was performed using LightCycler 480 SYBR Green I Master RT-PCR kit (Roche). Primer pairs used for RT-PCR experiments are provided in Supplementary Table 5. Signals were normalized to GAPDH and to control-transfected cells. Values represent relative mRNA abundance. Using a depletion cutoff set to 60% reduction in mRNA levels, the correlation between depletion and effects on autophagosome number is 75% (67 out of 96). For data obtained by immunoblotting, there was a 79% correlation (19 out of 24).

Data processing and initial analysis. Mass spectral data were processed using CompPASS, as previously described⁹ with modifications. Sequest summary files were processed into a high threshold data set based on a 2% protein false-positive rate as described earlier⁹. These processed data sets were merged for each duplicate run and used to populate a ‘stats table’ consisting of each data set for the AIN as well as 102 unrelated proteins (Dubs and their selected HCIPs; https://harper.hms.harvard.edu/CompPASS_Dubs.html). The D^N- and Z-scores were calculated from total spectral counts (TSCs) for each protein found in association with each bait. Because CompPASS was originally designed for analysis of mostly non-reciprocal data sets⁹, we devised a new weighted D^N-score (WD^N-score) (Supplementary Fig. 2), which aids in the identification of HCIPs that are associated with multiple baits in a network. Proteins identified in each LC-MS/MS experiment with a WD^N-score ≥ 1 and a *P*-value ≤ 4.9 × 10⁻⁶ are considered to be HCIPs.

Additional bioinformatic analysis. Interactions used for generating protein networks were from the STRING database, found at <http://string.embl.de/>; the BioGRID database found at <http://www.thebiogrid.org/downloads.php>; and the MINT database found at <http://mint.bio.uniroma2.it/mint/download.do>. When necessary, Ensembl nomenclature was converted into NCBI gene symbols using Ensembl’s BioMart (<http://www.ensembl.org/biomart/index.html>). Output files from CompPASS for network analysis are in the ‘sif’ format, which is compatible with Cytoscape (<http://www.cytoscape.org>), and additional files containing both node and edge attributes are generated. Attribute files were used in Cytoscape to assign values for nodes and edges, as indicated. Gene Ontology (GO) process terms were analysed in CompPASS, essentially as described⁹.

Pfam analysis was performed in-house using HMMER software and the Pfam_ls set of Hidden Markov matrices from <ftp://ftp.sanger.ac.uk/pub/databases/Pfam/>. All clustering was done using Multiple Experiment Viewer (<http://www.tm4.org/mev.html>) and protein interaction maps were generated using Cytoscape (<http://www.cytoscape.org>).

Comparison of HCIP abundance. To compare the abundance of HCIPs found in the wild-type and mutant ATG8 protein IP-MS/MS experiments, and in experiments examining the effect of Torin1 on subnetworks, we used the normalized spectral abundance factor (NSAF) approach previously applied to determine the abundance of proteins found in IP-MS/MS data sets¹⁶. For each interactor in each IP-MS/MS experiment, the NSAF was calculated and then difference in NSAF values for that protein in wild-type control and mutant experiments was determined (see Supplementary Methods for detailed formulas). To plot the data using the log₂ values of this difference while maintaining the proper sign of the value (positive for increase and negative for decrease), the conventional NSAF was multiplied by 100,000 so that each value was ≥ 1 before taking the log₂ of the difference.

37. Thorrein, C. C. et al. An ATP-competitive mammalian target of rapamycin inhibitor reveals rapamycin-resistant functions of mTORC1. *J. Biol. Chem.* 284, 8023–8032 (2009).
38. Shvets, E. & Elazar, Z. Flow cytometric analysis of autophagy in living mammalian cells. *Methods Enzymol.* 452, 131–141 (2009).